ARTICLE

CCDC115 Deficiency Causes a Disorder of Golgi Homeostasis with Abnormal Protein Glycosylation

Jos C. Jansen,[1,2,28] Sebahattin Cirak,[3,4,5,28] Monique van Scherpenzeel,[2,6] Sharita Timal,[2,6] Janine Reunert,[7] Stephan Rust,[7] Belén Pérez,[8] Dorothée Vicogne,[9] Peter Krawitz,[10] Yoshinao Wada,[11] Angel Ashikov,[2,6] Celia Pérez-Cerdá,[8] Celia Medrano,[8] Andrea Arnoldy,[12] Alexander Hoischen,[13] Karin Huijben,[2] Gerry Steenbergen,[2] Dulce Quelhas,[14] Luisa Diogo,[15] Daisy Rymen,[16] Jaak Jaeken,[16] Nathalie Guffon,[17] David Cheillan,[17] Lambertus P. van den Heuvel,[2,18] Yusuke Maeda,[19] Olaf Kaiser,[20] Ulrike Schara,[20] Patrick Gerner,[21] Marjolein A.W. van den Boogert,[22] Adriaan G. Holleboom,[22] Marie-Cécile Nassogne,[23] Etienne Sokal,[23] Jody Salomon,[1] Geert van den Bogaart,[24] Joost P.H. Drenth,[1] Martijn A. Huynen,[25] Joris A. Veltman,[13,26] Ron A. Wevers,[2] Eva Morava,[16,27] Gert Matthijs,[16] François Foulquier,[9,28] Thorsten Marquardt,[7,28] and Dirk J. Lefeber[2,6,28,*]

Disorders of Golgi homeostasis form an emerging group of genetic defects. The highly heterogeneous clinical spectrum is not explained by our current understanding of the underlying cell-biological processes in the Golgi. Therefore, uncovering genetic defects and annotating gene function are challenging. Exome sequencing in a family with three siblings affected by abnormal Golgi glycosylation revealed a homozygous missense mutation, c.92T>C (p.Leu31Ser), in coiled-coil domain containing 115 (*CCDC115*), the function of which is unknown. The same mutation was identified in three unrelated families, and in one family it was compound heterozygous in combination with a heterozygous deletion of *CCDC115*. An additional homozygous missense mutation, c.31G>T (p.Asp11Tyr), was found in a family with two affected siblings. All individuals displayed a storage-disease-like phenotype involving hepatosplenomegaly, which regressed with age, highly elevated bone-derived alkaline phosphatase, elevated aminotransferases, and elevated cholesterol, in combination with abnormal copper metabolism and neurological symptoms. Two individuals died of liver failure, and one individual was successfully treated by liver transplantation. Abnormal N- and mucin type O-glycosylation was found on serum proteins, and reduced metabolic labeling of sialic acids was found in fibroblasts, which was restored after complementation with wild-type *CCDC115*. PSI-BLAST homology detection revealed reciprocal homology with Vma22p, the yeast V-ATPase assembly factor located in the endoplasmic reticulum (ER). Human CCDC115 mainly localized to the ERGIC and to COPI vesicles, but not to the ER. These data, in combination with the phenotypic spectrum, which is distinct from that associated with defects in V-ATPase core subunits, suggest a more general role for CCDC115 in Golgi trafficking. Our study reveals CCDC115 deficiency as a disorder of Golgi homeostasis that can be readily identified via screening for abnormal glycosylation in plasma.

Introduction

Congenital disorders of glycosylation (CDGs) are a heterogeneous group of monogenic diseases affecting the glycosylation of proteins and lipids. Approximately 100 CDGs have been described so far, and they affect multiple glycosylation pathways.[1] CDGs with abnormal protein N-linked glycosylation can be divided into type 1 CDGs, affecting glycan assembly in the endoplasmatic reticulum (ER), and type 2 CDGs, affecting glycan modification in the Golgi apparatus. Identification of disease-associated genes in the latter group is complicated by the complexity of

[1]Department of Gastroenterology and Hepatology, Radboud University Medical Center, 6525 GA Nijmegen, the Netherlands; [2]Translational Metabolic Laboratory, Radboud Institute for Molecular Life Sciences, Radboud University Medical Center, 6525 GA Nijmegen, the Netherlands; [3]Institut für Humangenetik, Uniklinik Köln, 50931 Köln, Germany; [4]Klinik und Poliklinik für Kinder- und Jugendmedizin, Uniklinik Köln, 50937 Köln, Germany; [5]Zentrum für Molekulare Medizin, Uniklinik Köln, 50931 Köln, Germany; [6]Department of Neurology, Donders Institute for Brain, Cognition and Behavior, Radboud University Medical Center, 6525 GA Nijmegen, the Netherlands; [7]Department of Pediatrics, Westfälische Wilhelms-Universität Münster, 48149 Münster, Germany; [8]Centro de Diagnóstico de Enfermedades Moleculares, Centro de Biología Molecular Severo Ochoa UAM-CSIC, Universidad Autónoma de Madrid, Campus de Cantoblanco and Centro de Investigación Biomédica en Red de Enfermedades Raras (CIBERER) and Instituto de Investigación Sanitaria (IdiPAZ), 28049 Madrid, Spain; [9]CNRS-UMR 8576, Structural and Functional Glycobiology Unit, Federation of Research Structural & Functional Biochemistry of Biomolecular Assemblies (FRABio), University of Lille, 59655 Villeneuve d'Ascq, France; [10]Institute for Medical Genetics, 13353 Berlin, Germany; [11]Osaka Medical Center and Research Institute for Maternal and Child Health, Izumi, Osaka 594-1101, Japan; [12]Department of Pediatrics, University of Essen, 45122 Essen, Germany; [13]Department of Human Genetics, Radboud University Medical Center, 6525 GA Nijmegen, the Netherlands; [14]Biochemical Genetics Unit, Centro de Genética Médica Jacinto de Magalhães, Centro Hospitalar do Porto, 4050-466 Porto, Portugal; [15]Metabolic Diseases Unit, Centro de Desenvolvimento da Criança, Hospital Pediátrico, Centro Hospitalar Universitário de Coimbra, 3000-609 Coimbra, Portugal; [16]Department of Pediatrics, University of Leuven, 3000 Leuven, Belgium; [17]Centre de Référence des Maladies Héréditaires du Métabolisme, Hôpital Femme Mère Enfant, 69677 Bron Cedex, France; [18]Nijmegen Center for Mitochondrial Disorders, Translational Metabolic Laboratory, Department of Pediatrics, Radboud University Medical Center, 6525 GA Nijmegen, the Netherlands; [19]Research Institute for Microbial Diseases, Osaka University, Suita, Osaka 565-0871, Japan; [20]Department of Pediatric Neurology, Children's Hospital Essen, 45122 Essen, Germany; [21]Department of Pediatric Gastroenterology, Hepatology and Endoscopy, University Hospital, 79110 Freiburg, Germany; [22]Department of Vascular Medicine, Academic Medical Center, 1105 AZ Amsterdam, the Netherlands; [23]Cliniques Universitaires Saint-Luc, Université Catholique de Louvain, 1200 Woluwe-Saint-Lambert, Belgium; [24]Department of Tumor Immunology, Radboud University Medical Center, 6525 GA Nijmegen, the Netherlands; [25]Center for Molecular and Biomolecular Informatics, Radboud University Medical Center, 6525 GA Nijmegen, the Netherlands; [26]Department of Clinical Genetics, Maastricht University Medical Centre, 6229 HX Maastricht, the Netherlands; [27]Hayward Genetics Center, Department of Pediatrics, Tulane University Medical School, New Orleans, LA 70112, USA
[28]These authors contributed equally to this work
*Correspondence: dirk.lefeber@radboudumc.nl
http://dx.doi.org/10.1016/j.ajhg.2015.12.010.

the Golgi apparatus and the heterogeneous phenotype of individuals with CDGs, making phenotypic clustering difficult. Type 2 CDGs can be further grouped on the basis of disease mechanism. Mutations in genes encoding for proteins directly involved in Golgi glycosylation (e.g., *SLC35A1* [MIM: 605634], *B4GALT1* [MIM: 137060], and *MGAT2* [MIM: 602616]) were the first to be discovered.[2–4] Another group of type 2 CDGs are caused by disturbances in Golgi homeostasis. This group encompasses several conserved oligomeric Golgi (COG)-CDGs, TMEM165-CDG (MIM: 614726) and ATP6V0A2-CDG (MIM: 611716). The COG complex is involved in retrograde Golgi transport, and mutations lead to abnormal distribution of proteins involved in the glycosylation machinery, such as glycosyltransferases.[5] *TMEM165* mutations were recently described in individuals with skeletal symptoms and linked with deficient Ca^{2+} and pH homeostasis.[6,7] *ATP6V0A2* mutations were described in autosomal-recessive cutis laxa type 2 (ARCL2 [MIM: 219200]).[8] *ATP6V0A2* encodes a subunit of the vacuolar H^+ ATPase (V-ATPase), which is primarily responsible for acidification of organelles within the secretory pathway and endolysosomal system.[9] Fibroblasts from ARCL2-affected individuals show delayed retrograde Golgi transport, in accordance with the versatile role of the V-ATPase and its involvement in multiple cellular processes.[10,11]

Traditionally, diagnostics for protein N-glycosylation defects is performed with isoelectric focusing (IEF) of serum transferrin (Tf). This method is used to distinguish between type 1 and type 2 CDGs.[12] Additionally, IEF of serum apolipoprotein C-III (ApoC-III) can detect abnormal mucin-type O-glycosylation.[13] Recently, we described the use of a high resolution nanochip-C8 QTOF mass spectrometry method for annotation of glycan structures on intact serum Tf.[14] This method provides additional glycan information, such as loss of galactose.

Here, we report the identification of pathogenic mutations in coiled-coil domain containing 115 (*CCDC115* [GenBank: NM_032357.3], UCSC Genome Browser [GRCh37/hg19], chr2:131,095,506–131,099,956) in five unrelated families with abnormal N- and mucin type O-glycosylation, suggestive of a Golgi homeostasis defect.

Material and Methods

Participating Individuals

Blood and, if obtained, fibroblasts of participating individuals were sent to the Radboud University Medical Center, Translational Metabolic Laboratory, for CDG diagnostics, based on clinical suspicion for an inborn error of metabolism. All participating affected individuals or their legal representatives gave informed consent for exome sequencing. Tissue and samples were obtained in accordance with the Declaration of Helsinki.

Exome Sequencing and Interpretation

Next-generation sequencing and analysis were performed as described earlier.[15] The SureSelect Human All Exon 50 Mb Kit (v.4, Agilent) was used for exome enrichment, covering ~21,000 genes. The exome library was sequenced on a 5500xl SOLiD sequencer (Life Technologies). Color space reads were iteratively mapped to the hg19 reference genome with the SOLiD LifeScope software v.2.1. We used our in-house annotation pipeline for annotation of called variants and indels.[16]

Variants were excluded based on a frequency of >0.2% in our in-house database of >1,300 exomes. Also, synonymous variants, deep intronic variants, and variants in UTRs were excluded. Quality criteria were applied and included variants called more than five times and with variation of more than 20% for heterozygous variants and 80% for homozygous variants.

Bioinformatics

Amino acid sequences of human CCDC115 and homologs of other species were aligned and visualized with Jalview v.2.8 (see Web Resources). The following accession numbers were used for the alignment in Figure 1B: GenBank: NP_115733.2 (*H. sapiens*); GenBank: NP_081435.1 (*M. musculus*); GenBank: NP_001013313.1 (*D. rerio*); GenBank: NP_649550.1 (*D. melanogaster*); GenBank: NP_011927.1 (*S. cerevisiae* S288c); GenBank: NP_173500.1 (*A. thaliana*).

Mutation Analyses

In silico analysis was done with Alamut v.2.4.6 (Interactive Biosoftware) and the effects of mutations were predicted with SIFT, PolyPhen, and MutationTaster (see Web Resources). The Exome Aggregation Consortium (ExAC) database (see Web Resources) was used for allele frequency.

Primers (Biolegio and Sigma-Aldrich) flanked with universal M13 tags were constructed with the help of the UCSC Genome Browser, Primer3, and SNPCheck3 (see Web Resources).[17,18] For a list of primers used, see Table S1. Sanger sequencing was performed on DNA isolated from peripheral blood or cultured fibroblasts, according to standard protocols. DNA was amplified with a T100 ThermoCycler (Bio-Rad). An ABI 3730 DNA Analyzer (Life Technologies) was used for sequencing. Data analysis was done with Sequencher 4.8 (Gene Codes).

Multiplex ligation-dependent probe amplification (MLPA) was performed as described previously.[19] In short, combinations of two adjacently annealing oligonucleotide probes were hybridized and ligated. After ligation, the common ends of the probes served as a template for PCR amplification with one primer pair, and due to the fluorescent labeling of the primer, the resulting products could be separated according to size via capillary electrophoresis on an ABI3130 Genetic Analyzer (Applied Biosystems). Fragment data were analyzed in GeneScan (Applied Biosystems). Peak heights of samples from affected individuals were compared with those from control individual probes, and ratios were calculated for all fragments (originating from *CCDC115*, *PTPN18*, and *SMPD4* exons) via an Excel spreadsheet. Thresholds for deletions and duplications were set at 0.75 and 1.25 respectively, and all samples were tested at least twice. All reagents for the MLPA reaction and subsequent PCR amplification were purchased from MRC-Holland, with exception of the *CCDC115*, *PTPN18*, *SMPD4*, and control primers (Biolegio). Primer sequences are described in Table S1.

Cell Culture

Skin fibroblasts from participants and healthy control individuals were cultured at 37.0°C under 5.0% CO_2 in culture medium E199, supplemented with 10% fetal calf serum, and 1%

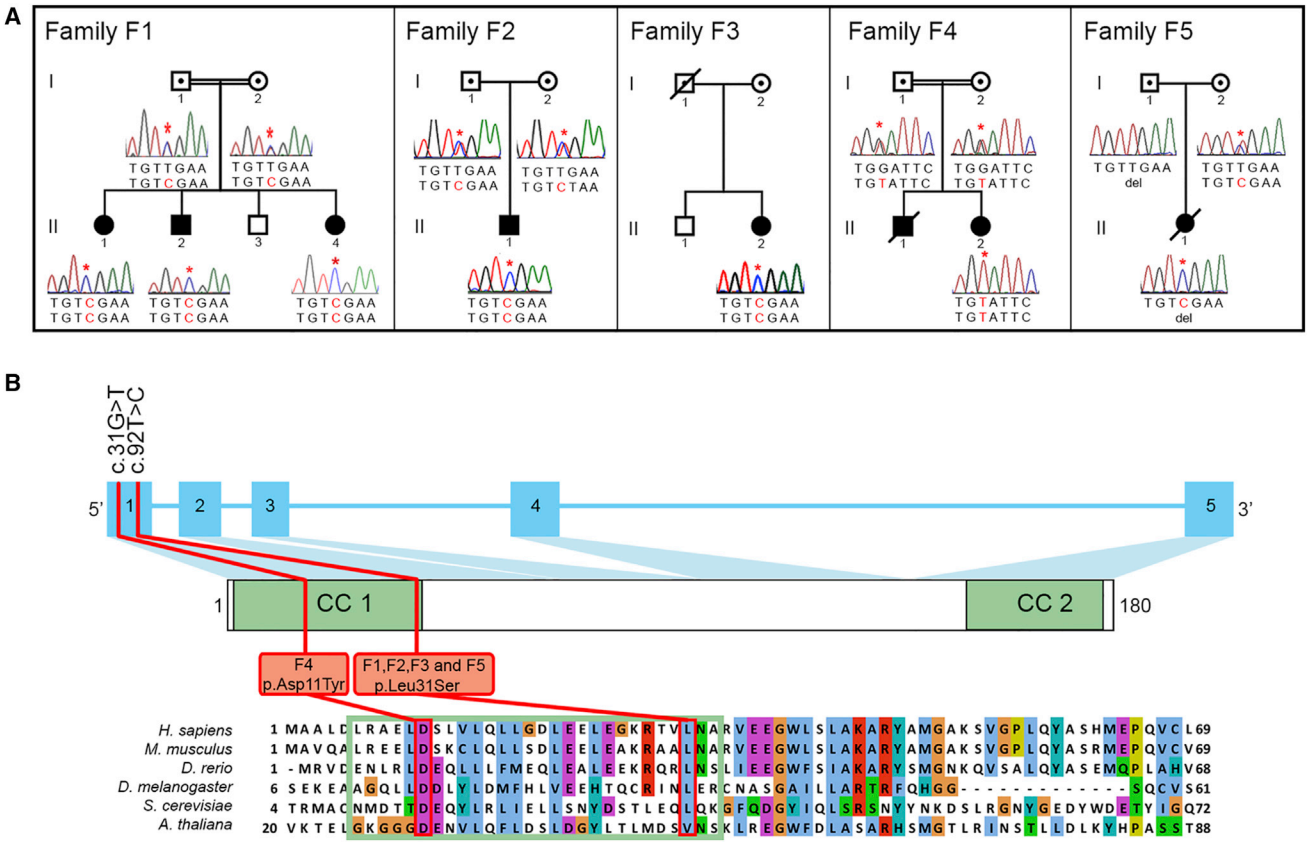

Figure 1. Pedigrees and Overview of the Structure, Variants, and Conservation of *CCDC115*

(A) Pedigrees and chromatograms of families F1 to F5 are shown. Partial chromatograms show autosomal-recessive segregation for all families. For family F3, DNA for parents and the healthy sibling was not available. For affected individual F4-II1, DNA was unavailable. The asterisk indicates the respective nucleotide change.

(B) Schematic representation of the intron-exon structure and homology of *CCDC115*. The red lines indicate the positions of the missense mutations and substitutions within the families. The green regions indicate the two predicted coiled-coil domains (CC1 and CC2).

penicillin/streptomycin. All cultures were tested for mycoplasma infection prior to cultivation.

Cloning Studies

CCDC115 Wild-Type Sequence in pLIB-GSKBrd for Transfection in Skin-Derived Fibroblasts

A retroviral pLIB construct was purchased from Clontech, and a PGK-Blasticidin resistant cassette was introduced to create a pLIB-PGKBsr vector. Human *CCDC115* was then cloned into this vector. Skin fibroblasts from individual F1-II4 were transfected with either pLIB2-pgkBsr construct (empty vector) or pLIB2-*CCDC115*-PGKBsr construct.

pcDNA3.1-CCDC115-V5-His for Transfection in HeLa cells

CCDC115 cDNA was obtained from healthy control fibroblasts with the Transcriptor First Strand cDNA Synthesis Kit (Roche) and primers spanning the whole cDNA (see Table S1 for primer sequences). cDNA was sequenced and cloned into the mammalian expression vector pcDNA3.1_V5_His TOPO-TA (Life Technologies). The construct was checked via Sanger sequencing and transformed in competent *E. coli*. DNA was extracted with the Birnboim method and checked for correct placement of the *CCDC115* strand.[20] Plasmid purification was done with the Plasmid Midi Kit (QIAGEN) according to the manual. Transfection was done with FuGENE HD Transfection Reagent (Promega) on coverslips coated with poly-L-Lysine (Sigma) and incubated overnight in DMEM (GIBCO) with 30%–50% confluency for immunofluorescence studies.

Immunofluorescence

48 hr after transfection of HeLa cells with pcDNA3.1-*CCDC115*-V5-His, cells were fixed with 3.7% paraformaldehyde (PFA) for 12 min, washed three times in PBS, and permeabilized with 0.1% Triton in 3% BSA/1× PBS at 4°C for 10 min. After washing in PBS, cells were blocked for 30 min with 3% BSA/1× PBS solution. Primary antibodies were diluted in 3% BSA/1× PBS. Cells were incubated with primary antibody in a wet environment for 1 hr at room temperature (RT) and, after washing with PBS, incubated for 1.5 hr with secondary antibodies in 3% BSA/1× PBS. After washing the cells three times with PBS and once with distilled water, they were mounted on a slide with Prolong Gold antifade with DAPI (Life Technologies) and left to dry at RT for at least 24 hr. Under identical settings, the cells were visualized with a confocal Leica SP8 (Leica Microsystems) with 60× water immersion and 1.2 NA objective. Picture processing was done with ImageJ software v.1.46 (see Web Resources). Primary antibodies used are as follows: anti-V5-Tag (1:200, Life Technologies, #R960-25), anti-beta COP (1:1,000, Abcam, #ab2899), anti-SEC31A (1:500, Sigma-Aldrich, #HPA005457), anti-Giantin (1:1,000, BioLegend, #prb-114c), anti-ERGIC53/p58 (1:200, Sigma-Aldrich, #E1031), anti-PDI (1:500, Abcam, #ab3672), anti-Calnexin (1:200, StressMarq Biosciences, #SPC-108). Secondary antibodies are as follows: Alexa Fluor 488-conjugated goat anti-mouse IgG (H+L) (1:1,000, Life Technologies, #A-11029) and Alexa Fluor 568-conjugated goat anti-rabbit IgG (H+L) (1:1,000, Life Technologies, #A-11011).

IEF of Tf and ApoC-III

Tf IEF was performed as previously described.[21] In short, 10 μl serum or plasma sample was added to a solution containing iron and $NaHCO_3$, electrophorized on a 5–7 pH gradient gel, and incubated with 60 μl polyclonal rabbit anti-Tf antibody (Dako, #A0061). Quantification of the gel was done with Image Quant software (TotalLab). Neuraminidase treatment was performed when a Tf polymorphism was suspected as described earlier.[21]

ApoC-III IEF was performed as described, but with small modifications.[13] In short, 2 μl of serum/plasma was 15× diluted with saline solution. Before electrophoresis, the gel was rehydrated in a solution containing 8 M urea. After blotting on a nitrocellulose membrane filter, the blot was washed and blocked before incubation with anti-ApoC-III (1:2,000, Rockland, #600-101-114). After incubation with the secondary anti-goat-HRP antibody (1:5,000, Thermo Scientific, #31402) and ECL reagent (Pierce), the blot was visualized on a LAS3000 imaging system (Fujifilm). Blot quantification was done with Image Quant software.

MALDI-LTQ Mass Spectrometry

Mass spectrometry of total plasma N-glycans was performed as described earlier.[22] To summarize, glycans from 10 μl plasma were cleaved with PNGaseF (NE Biolabs) and incubated overnight. After purification on graphitized carbon SPE columns, the glycans were permethylated, purified again, and eluted in 50 μl of 75% v/v aqueous acetonitrile. The glycans were dried and resuspended in a methanol/sodium acetate mixture for spotting. Measurements were done on a vMALDI-LTQ (Thermo Scientific).

Nanochip-C8 QTOF Mass Spectrometry of Intact Tf

For high-resolution mass spectrometry of the intact Tf protein, 10 μl of serum sample was incubated with anti-Tf beads before injection, and the eluate was analyzed on a microfluidic nanoLC-C8-chip 6540 QTOF instrument (Agilent Technologies).[14] Agilent Mass Hunter Qualitative Analysis Software B.04.00 was used for data analysis. For deconvolution of the charge distribution raw data, Agilent BioConfirm Software was used.

Metabolic Labeling with Alkyne-Tagged Modified Sugar

Metabolic labeling was performed as described before.[23] Primary skin fibroblasts were maintained in DMEM supplemented with 10% fetal bovine serum (Lonza), at 37°C under 5% CO_2 atmosphere. Fibroblasts were grown overnight on glass coverslips (12 mm diameter). Medium was then changed with pre-warmed medium containing 500 μM of alkynyl-modified sugar (ManNAl, provided by Dr. Y. Geurardel and Prof. C. Biot). Labeling lasted 8 hr or 6 hr. The labeling was stopped by fixing the cells with 4% PFA. Cells were then permeabilized in 0.5% Triton X-100 for 10 min. After washes, cells were incubated in the click chemistry buffer containing CuSO4, 5H2O-BTTAA-ascorbate-potassium phosphate, and azide-fluor 545 (Sigma, #760757). The pool of fluorescent glycoconjugates was visualized through an inverted Leica TCS-SP5 confocal microscope. Pictures were taken with the Leica Application Suite Advanced Fluorescence (LAS AF) software (Leica Microsystems). For comparison purposes, each picture was taken under the same settings. TISGolgi was used to automatically detect the Golgi area and measure the Golgi fluorescence. This homemade ImageJ plugin was developed by TISBio (see Web Resources). Three different fields of two independent experiments were examined.

Results

Clinical Phenotype

All affected individuals (see pedigrees in Figure 1A and overview in Table 1) had a similar phenotype with storage-disease-like symptoms at a younger age. These included hepatosplenomegaly, hypotonia, elevated serum aminotransferases (ATs, composed of aspartate and alanine aminotransferases [AST, ALT]), and elevated serum alkaline phosphatase (ALP). Additional symptoms included psychomotor disability (PMD), mild hypercholesterolemia, and low serum ceruloplasmin.

Siblings F1-II1 (female, born in 2000) and F1-II2 (male, born in 2004) from family F1 were from Turkish ancestry and have been described previously.[24] Their parents are first cousins. During our studies, a younger affected sister was born (individual F1-II4, female, born in 2012). Overall, their symptoms were dominated by PMD, hypotonia, and hepatosplenomegaly with elevated AT and ALP. Metabolic screening revealed a type 2 CDG profile. Individual F1-II1 was first seen at the age of nine years. Her neonatal period was unremarkable. At examination there was a generalized hypotonia and PMD. She showed mild dysmorphic features. Over the years her AT and ALP fluctuated but were always elevated (AST 130–158 U/l [normal range, 0–50 U/l], ALT 85–101 U/l [normal range, 0–50 U/l], and ALP 1,016 –1,193 U/l [normal range, < 360 U/l]). Isotype analysis showed that ALP was mostly bone derived, as seen in defects of glycosylphosphatidylinositol (GPI)-anchor biosynthesis. However, surface expression of GPI-anchored proteins CD59 and CD55 in EBV-transformed lymphoblasts did not confirm a GPI-anchor defect (data not shown). Additional biochemical analysis showed low serum ceruloplasmin (4 mg/dl [normal range, 15–60 mg/dl]), decreased coagulation factors, and elevated creatine kinase. Total cholesterol and low-density lipoprotein (LDL-C) were normal. Her brother, F1-II2, was also seen in 2009 at the age of five years. He shared the same phenotype as his sister but had additional dysmorphic features (long face, ptosis, blue sclera, and down-slanting palpebral fissures). In addition to generalized hypotonia, muscle atrophy was present. Biochemically, elevated AT and ALP (AST 96–436 U/l, ALT 140–995 U/l, and ALP 1,070–1,577 U/l), low ceruloplasmin (4 mg/dl), hypercholesterolemia (289 mg/dl [normal range, 120–200 mg/dl]), and abnormal coagulation factors were seen over time. Individual F1-II4 was last seen in 2014 at the age of two years. The most prominent finding was PMD. Hypotonia was not present. Hepatic evaluation showed elevated AST (1,089 U/l), ALT (591 U/l), ALP (1,251 U/l), and profound hepatosplenomegaly, similar to lysosomal storage disorders in the first years of life. Organ size normalized with increasing age.

Individual F2-II1 (male, born in 2008) from family F2 was the only child of unrelated Italian parents. As a neonate, he suffered from prolonged neonatal jaundice and elevated AST, ALT, and hepatosplenomegaly. Low serum ceruloplasmin and hypercholesterolemia were

Table 1. Overview of the Genetic and Clinical Features of the CCDC115-Deficient Families

Family	Individual (y.o.b.)	Zygosity	Allele Frequency (ExAC)	gDNA Change (chr2)	cDNA Change	Protein Change	Abnormal Glycosylation		Elevated ATs	Elevated ALP	Elevated Cholesterol and LDL-C	Cerulo plasmin	Hepatic Phenotype	Neurological Phenotype
							N	O						
F1	F1-II1 (2000), F1-II2 (2004), F1-II4 (2012)	homozygous	8.253e-06	g.131099607A>G	c.[92T>C]; [92T>C]	p.[Leu31Ser]; [Leu31Ser]	+	+	+	++	+	low	hepatomegaly	hypotonia, PMD
F2	F2-II1 (2008)	homozygous	8.253e-06	g.131099607A>G	c.[92T>C]; [92T>C]	p.[Leu31Ser]; [Leu31Ser]	+	+	+	++	+	low	hepatomegaly, copper accumulation	PMD
F3	F3-II2 (1989)	homozygous	8.253e-06	g.131099607A>G	c.[92T>C]; [92T>C]	p.[Leu31Ser]; [Leu31Ser]	+	n.d.	+	++	+	low	fibrosis, steatosis, necrotic lesions	hypotonia, PMD, seizures
F4[a]	F4-II1 (2002), F4-II2 (2003)	homozygous	0	g.131099668C>A	c.[31G>T]; [31G>T]	p.[Asp11Tyr]; [Asp11Tyr]	+	+	+	++	+	n.d.	liver failure[b]	–
F5[c]	F5-II1 (2014)	compound heterozygous	8.253e-06 / NA	g.131099607A>G / g.(130939272_131096872)_(131116671_?)del	c.[92T>C]; [(?_-258)_(*1245_?) del]	p.[Leu31Ser]; [p.0?]	+	+	+	++	+	n.d.	hepatomegaly, cirrhosis, liver failure	hypotonia

Abbrevations are as follows: y.o.b., year of birth; N, N-glycosylation measured by IEF of serum Tf; O, O-glycosylation measured by IEF of serum ApoC-III; LDL-C, low-density lipoprotein; ATs, serum aminotransferases; ALP, serum alkaline phosphatase; PMD, psychomotor disability; n.d., not determined; NA, not applicable.
[a]Sibling F4-II1 died at the age of 9 years as a result of liver failure after repeated liver transplantation.
[b]Both siblings underwent liver transplantation.
[c]Individual F5-II1 died of liver failure at the age of 7 months.

found. On suspicion of Wilson disease (WD [MIM: 277900]), zinc treatment was started but proved unsuccessful. Genetic screening for WD failed to detect mutations in *ATP7B* (MIM: 606882). At the age of two years, examinations showed mild PMD and mild dysmorphic features. Biochemical analysis revealed elevated AT and ALP (AST 422 U/l, ALT 588 U/l, ALP 976 U/l), low ceruloplasmin (3.3 mg/dl), high cholesterol (381 mg/dl), and high LDL-C (332 mg/dl [normal range, 50–130 mg/dl]). Metabolic diagnostics showed a type 2 CDG pattern. A liver biopsy at the age of three years showed an increased hepatic copper concentration of 125 μg/g dry weight (normal range, <40 μg/g dry weight; WD, >250 μg/g dry weight).

Individual F3-II2 (female, born in 1989) from family F3 was the second child of unrelated French parents. She had an uncomplicated birth but developed neonatal jaundice, which was treated successfully by phototherapy. This was accompanied by elevated AT and ALP. She was hospitalized at the age of one year due to persistent moderate hypotonia. Biochemically, she had elevated AST (1,780 U/l), ALT (390 U/l), and ALP (950 U/l, with increased bone fraction). Steatosis, fibrosis, and necrotic lesions were seen on liver biopsy. During childhood, she developed PMD with hypotonia and seizures. Biochemically, elevated AT and ALP persisted. At a later age, she developed hypercholesterolemia. CDG screening showed a type 2 pattern. During her last visit at the age of twenty-five years, she still suffered from PMD, as well as additional behavioral problems such as aggressiveness, agitation, and psychotic behavior, for which she is being treated with risperidone. Her seizures persisted despite treatment with lamotrigine. Serum AT and ALP remain elevated (AST 82 U/l, ALT 76 U/l, ALP 180 U/l) and ceruloplasmin low (10 mg/dl).

Individuals F4-II1 (male, born in 2002, died in 2011) and F4-II2 (female, born in 2003) are brother and sister and were born to consanguineous Turkish parents. As a neonate, individual F4-II1 showed neonatal jaundice. Progressive cholestatic liver disease was diagnosed at an early age. Due to progressive liver failure, sibling F4-II1 underwent a liver transplantation at the age of three years and ten months, and sibling F4-II2 at the age of eight years. Unfortunately, the transplant of sibling F4-II1 was rejected twice, and he died at the age of nine years. Both siblings showed mild dysmorphic features and individual F4-II1 had a mild PMD. They showed elevated AT and ALP during several check-ups (F4-II1: AST 192–669 U/l, ALT 83–308 U/l, ALP 702 U/l; F4-II2: AST 98–422 U/l, ALT 98–178 U/l, ALP 710–985 U/l). Ceruloplasmin was never measured. After liver transplantation, individual F4-II2 is doing well. Among other parameters, her AT and CDG profile have normalized.

Individual F5-II1 (female, born in 2014, died after seven months) was the only child of non-consanguineous Portuguese parents. Jaundice was noticed since the first day of life. At five months, jaundice persisted and she developed hepatosplenomegaly, failure to thrive, redundant skin, poor muscle volume, and generalized hypotonia. There were no signs of PMD. Her parents refused a liver biopsy. Intermittent episodes of hypoglycemia and hyperammonemia ensued. Subsequently, she developed progressive cholestatic liver disease (bilirubin 41.3 mg/dl, 40% conjugated) and liver failure. Investigation showed increased ATs (AST 207–972 U/l, ALT 48–153 U/l) and ALP (850–1,031 U/l). Additional biochemical analysis revealed hypercholesterolemia (431 mg/dl) and elevated LDL-C (314 mg/dl), abnormal coagulation factors (low FVII and high FVIII, INR 0.79–3.0), and anemia (Hb 7 g/dl) with acanthocytes and 7% reticulocytes. Interestingly, a bone marrow biopsy showed dyserythropoiesis, some lipidic histiocytes, and erythrophagocytosis. Later on, generalized cell vacuolization and few erythroblasts with perinuclear deposition of iron were seen. CDG screening revealed a type 2 pattern. Liver transplantation was not attempted due to rapid deterioration with multi-organ failure and encephalopathy. She died at the age of seven months. Postmortem liver analysis revealed severe cholestatic hepatitis with complete septal fibrosis and cirrhosis.

Mutational Analyses

To uncover the genetic defect, we performed exome sequencing of individuals F1-II1 and F1-II2 from index family F1. Eight possible candidates were identified on the basis of having autosomal-recessive inheritance (Table S2). Among these candidates was a homozygous missense variant in *CCDC115* (c.92T>C [p.Leu31Ser]) (Table 1). We performed a profile-based method, Position-Specific Iterated (PSI)-BLAST,[25] to identify possible homologs of the candidate variants and identified Vma22p (GenBank: NP_011927.1) as the yeast homolog of CCDC115 (GenBank: NP_115733.2) in the second iteration with an E-value of 2e-14 and a reciprocal E-value of 3e-11. Vma22p is a dedicated ER-localized assembly factor of the V-ATPase.[9,26,27] Importantly, Vma22p and CCDC115 were found as each others' best hits. This suggests that, apart from being homologs, they are likely orthologs with overlapping functions in humans.[28] Based on the link between the V-ATPase and abnormal glycosylation, this variant was considered our most likely candidate.[7] This was further supported by homozygosity mapping, indicating a small homozygous region on chromosome 2, in which *CCDC115* was located (Figure S1). In silico analysis of the p.Leu31Ser substitution with SIFT, PolyPhen-2, and MutationTaster predicted pathogenicity (Table S3). The ExAC database showed a very low allele frequency of 8.253e-06. Sanger sequencing confirmed homozygosity for the affected individuals, heterozygosity for both parents, and homozygous wild-type sequence for a healthy sibling, confirming complete segregation in the family (Figure 1A). Western blotting of fibroblasts derived from individual F1-II4 demonstrated a protein level similar to that of healthy control individuals (Figure S2).

For individuals F2-II1 and F5-II1, exome sequencing revealed multiple genetic variants, among which was the same c.92T>C homozygous missense variant (Table 1). Sanger sequencing for individual F2-II1 confirmed homozygosity and heterozygosity for the parents (Figure 1A).

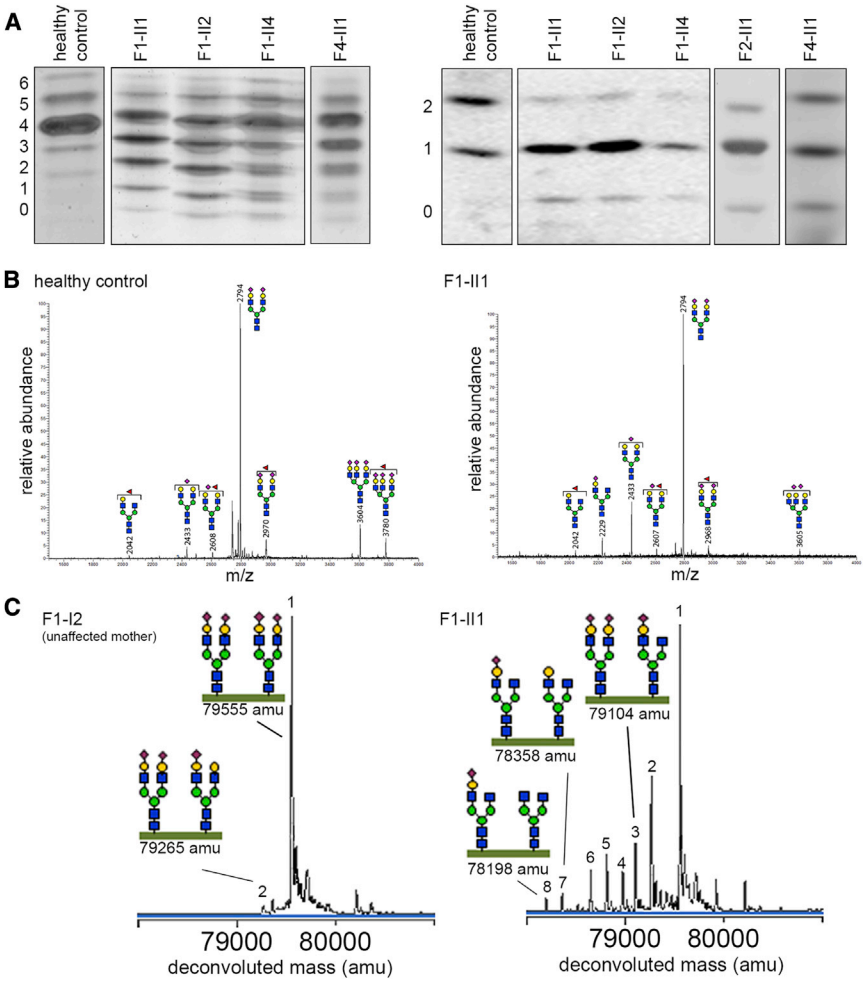

Figure 2. CCDC115-Deficient Individuals Have Abnormal Golgi Glycosylation
(A) IEF of serum Tf (left) and serum ApoC-III (right). For individual F2-II1, HPLC was used to assess Tf glycosylation status. Reference ranges and quantifications are shown in Tables S5 and S6.
(B) MALDI-LTQ mass spectrometry profiles of total serum N-glycans of a representative healthy control individual and of individual F1-II1. An increase in hypoglycosylated glycans with loss of sialic acid (purple diamond) and galactose (yellow dot) can be seen for individual F1-II1.
(C) For individual F1-II1 and his unaffected mother, nanochip-C8 QTOF mass spectra are shown for the intact Tf protein (including two attached glycans) at 79,555 amu (peak 1). Any subsequent loss of sialic acid and/or galactose can be calculated on the basis of mass difference with the main peak. Individual F1-II1 shows a reduction in sialic acid and galactose residues (peaks 2–8, see Table S7 for glycan structures). m/z, mass-to-charge ratio; amu, atomic mass units.

For individual F5-II1, Sanger sequencing of parental DNA revealed a maternal heterozygous missense mutation and a paternal wild-type sequence (Figure 1A). We suspected a paternal deletion as possible explanation, given that haplotype analysis excluded non-paternity. MLPA of DNA from individual F5-II1 displayed a heterozygous deletion for all exons of *CCDC115* and on the studied position in upstream *PTPN18* (Table S4). We did not observe a deletion for the position we investigated within downstream *SMPD4*. Segregation analysis showed that the deletion originated from the paternal allele. This complete deletion of *CCDC115* is in agreement with the severe phenotype of individual F5-II1.

Sanger sequencing of additional individuals with unsolved Golgi glycosylation defects identified missense mutations in *CCDC115* in individuals from two unrelated families: individual F3-II2 with the same homozygous c.92T>C mutation and siblings F4-II1 and F4-II2 with a homozygous missense mutation, c.31G>T, leading to a p.Asp11Tyr substitution (Figure 1A and Table 1). The p.Asp11Tyr substitution was also predicted to be pathogenic by SIFT, PolyPhen-2, and MutationTaster (Table S3). The allele frequency in the ExAC database was 0. In total, we found two missense mutations and one deletion in eight individuals from five families.

CCDC115 is located on the negative strand, contains five exons, and encodes coiled-coil domain containing 115 with 180 amino acids and two predicted coiled-coil domains (Figure 1B). Both *CCDC115* missense mutations are located in the first predicted coiled-coil domain and affect highly conserved positions. CCDC115 is widespread among eukaryotes, including *Arabidopsis thaliana*, indicating its origin at the root of the eukaryotic tree.

Glycosylation Studies

Global defects in glycosylation can be detected by IEF of serum Tf (N-glycosylation) and serum ApoC-III (mucin-type O-glycosylation). Tf has two N-glycosylation sites, and the most abundant fraction corresponds with four sialic acids. ApoC-III has one mucin-type O-linked glycan that can host one or two sialic acids. An increase in fractions associated with hyposialylated Tf or ApoC-III is indicative of abnormal N- or O-glycosylation. All individuals showed a similarly abnormal type 2 N-glycosylation profile of Tf (see Figure 2A and Table S5 for quantifications). ApoC-III IEF was abnormal for all tested individuals (see Figure 2A and Table S6 for quantifications).

We performed MALDI-LTQ mass spectrometry of total plasma N-glycans of individual F1-II1 and compared the spectrum with that of a healthy control individual. Most notably, the glycans with theoretical masses of 2,433 m/z and 2,229 m/z were increased, indicating loss of either one sialic acid (2,433 m/z) or one sialic acid plus one galactose (2,229 m/z) (Figure 2B).

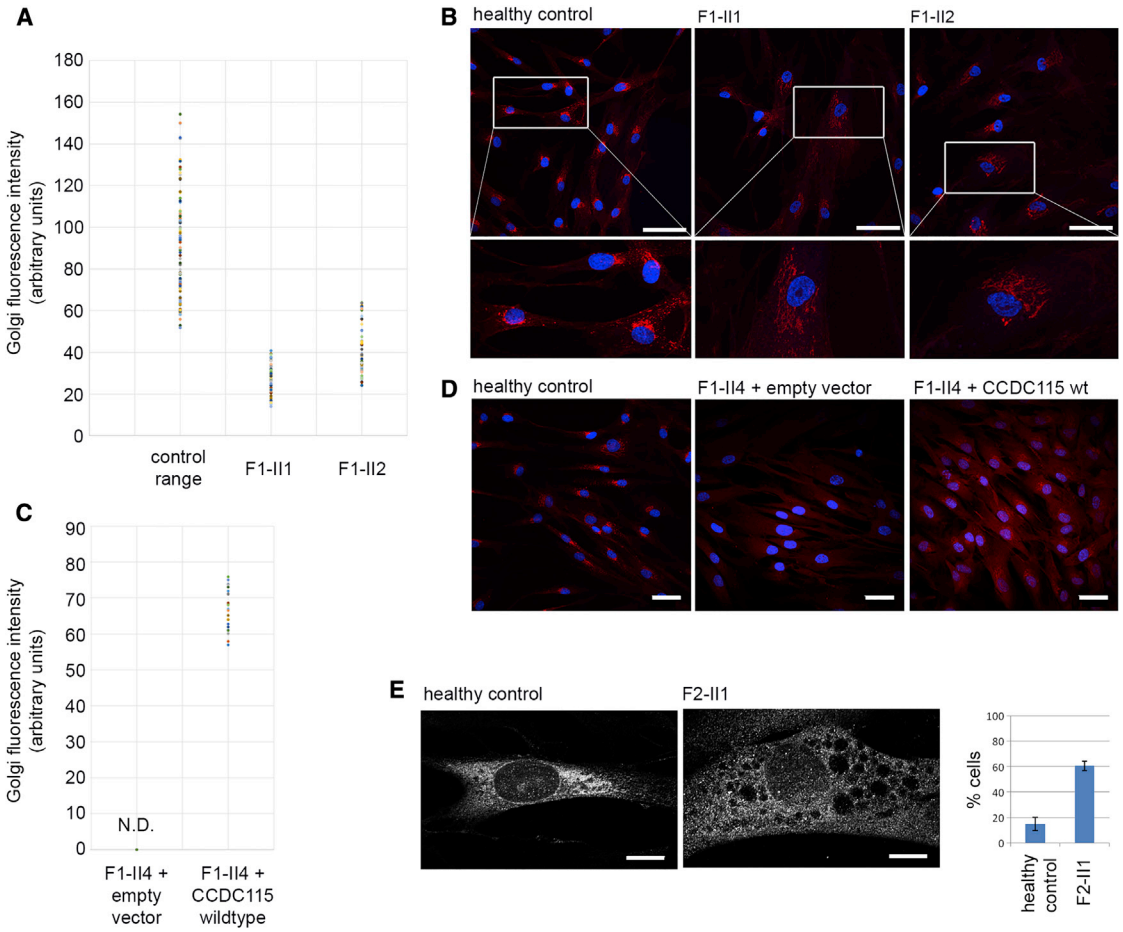

Figure 3. Metabolic Labeling of Sialic Acids Shows Decreased Glycosylation in CCDC115-Deficient Fibroblasts
(A and B) Metabolic labeling of fibroblasts with alkynyl-tagged sialic acid precursor ManNAl for 8 hr. Fibroblasts from three healthy controls were used, and the experiment was performed twice. A reduced absolute Golgi fluorescence signal was observed for siblings F1-II1 and F1-II2. Scale bars indicate 75 μm.
(C and D) Fibroblasts of F1-II4, transfected with empty vector or wild-type *CCDC115*, were incubated with ManNAl for 6 hr, followed by fluorescent staining. The graphs indicate the absolute Golgi fluorescence intensity in a.u. Scale bars indicate 50 μm.
(E) Healthy control fibroblasts and fibroblasts from CCDC115-deficient individual F2-II1 were stained with anti-calnexin antibody. The graph shows the percentage of cells with a dilated ER. Approximately 50 cells were counted, and the experiment was performed twice. The graph shows the percentage of cells (mean ± SEM) with a dilated ER. Scale bars indicate 10 μm. N.D., not detectable.

In accordance with total plasma N-glycan analysis, nanochip-C8 QTOF mass spectrometry of intact serum Tf (79,555 amu, peak 1) showed accumulation of incomplete glycans lacking sialic acid (79,265 amu, peak 2), galactose (79,104 amu, peak 3), and additional minor isoforms lacking sialic acid and/or galactose in individual F1-II1 (Figure 2C, peaks 4–8, see Table S7 for a list of all annotated glycan structures). This pattern is compatible with an overall detrimental effect on Golgi glycosylation. Together with abnormal O-glycosylation, these data are suggestive of a Golgi homeostasis defect and a combined disorder of N-glycosylation and mucin-type O-glycosylation.

Metabolic Labeling of Sialic Acids

We further assessed glycosylation efficiency in skin-derived fibroblasts by metabolic labeling of sialic acids with alkyne-tagged synthetic sugar analogs. These alkyne-tagged sialic acids are incorporated into nascent glycoproteins by the cell allowing for specific detection with fluorescently labeled azides.[23] In CCDC115-deficient individuals F1-II1 and F1-II2, the pool of glycoconjugates was located to the Golgi, and immunofluorescence signal quantification in the Golgi showed a clear reduction for all individuals, in agreement with less efficient Golgi glycosylation (Figures 3A and 3B). Additionally, we observed a dispersed pattern of the glycoconjugates, suggestive of dilatation of the Golgi (Figure 3B).

To investigate whether we could rescue the phenotype of individual F1-II4, we transfected skin fibroblasts with a construct containing either a mock construct or *CCDC115* wild-type sequence. As seen in Figures 3C and 3D, fibroblasts transfected with a mock construct have a non-detectable fluorescence intensity in the Golgi, in contrast to fibroblasts transfected with a construct containing wild-type *CCDC115*.

In addition to metabolic labeling, we stained healthy control fibroblasts and fibroblasts from affected individual

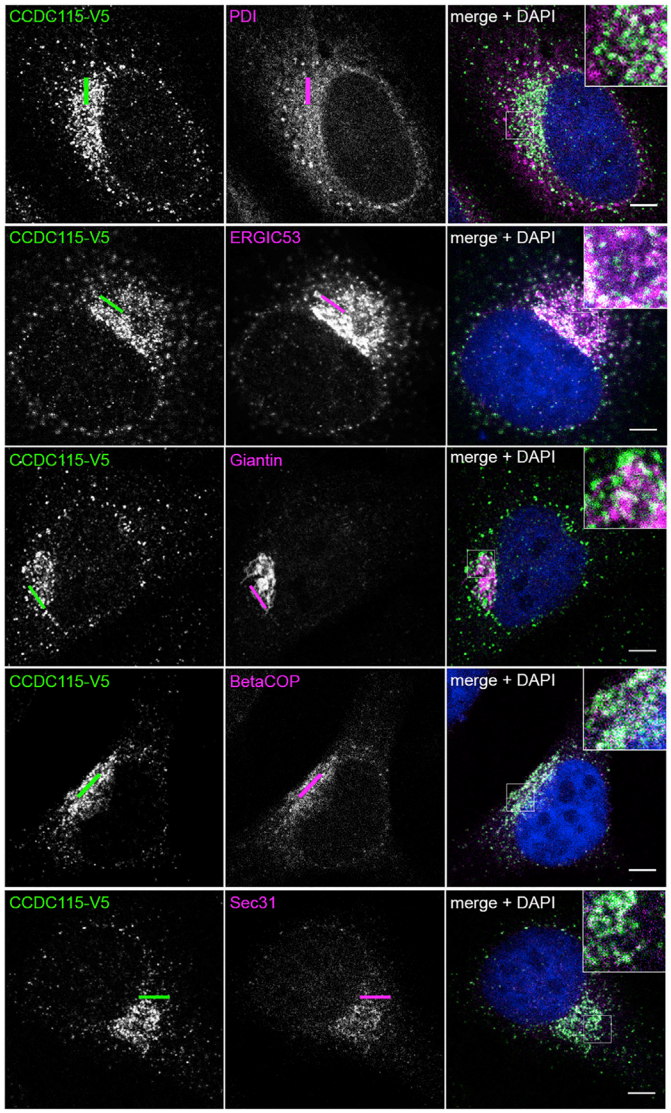

Figure 4. CCDC115-V5 Is Located in the ER-to-Golgi Region

HeLa cells were transiently transfected with a V5-tagged *CCDC115* construct and then fixed and stained with immunofluorescently labeled antibodies against V5 (green in merge) and different organelle markers (magenta in merge). Shown are representative cells stained for CCDC115-V5, organelle markers, and a merge with DAPI stain (blue), including a 3-fold magnification. Co-localization is indicated by white color in the merged channel. The graphs show the fluorescence intensity profiles along the cross-sections indicated. Scale bars represent 5 μm.

F2-II1 with anti-calnexin antibody to visualize the ER (Figure 3E). Individual F2-II1 fibroblasts showed a dilated ER in 60% of counted cells, in comparison to 20% in healthy control fibroblasts.

Localization

To define the subcellular location of CCDC115, we constructed a pcDNA3.1-*CCDC115*-V5 plasmid for transient expression of C-terminally V5-tagged CCDC115 in HeLa cells. Confocal imaging revealed clear localization to the ER-Golgi intermediate compartment (ERGIC) and coat protein complex I (COPI) vesicles (Figure 4). Also, in immortalized human hepatocytes (HepaRG), CCDC115 located to the ERGIC and COPI vesicles (data not shown). Partial co-localization was seen in both cell types with COPII and Golgi markers. No co-localization was seen with the ER marker PDI (Figure 4). We conclude that CCDC115 predominantly localizes to the ER-to-Golgi region but not to the ER, in contrast to yeast Vma22p.

Discussion

We identified *CCDC115* mutations in eight individuals from five unrelated families, and we provide evidence that these mutations affect protein N- and mucin-type O-glycosylation via their effect on Golgi homeostasis. Also, we showed that CCDC115 is localized to the ER-to-Golgi region. However, the question remains—what is the function of CCDC115 and how does its deficiency result in abnormal protein glycosylation and clinical symptoms?

Previous studies in mice suggest localization of CCDC115 to the lysosomal-endosomal system and upregulation of *Ccdc115* in mouse cortical neurons after fibroblast growth factor 2 (FGF2) stimulation.[29] Overexpression of *Ccdc115* in mouse embryonic fibroblasts has been shown to have a positive effect on cell proliferation.[30] Our data suggest a physiological role for CCDC115 in Golgi homeostasis, and loss-of-function mutations lead to the inability of the Golgi to perform its core functions: post-translational modification and protein secretion and sorting. A disturbance in Golgi homeostasis is indicated by the combined defect of N- and O-glycosylation. Detailed structural studies on N-glycans revealed an accumulation of incomplete glycans lacking both sialic acid and galactose. These data indicate a general disturbance in Golgi homeostasis with an effect on multiple glycosylation pathways, for example, via incorrect targeting and/or recycling of glycosyltransferases and nucleotide-sugar transporters. Previously, deficient vesicular transport has been proposed as explanation for abnormal Golgi glycosylation in COG and ATP6V0A2 defects.[5,10] Localization of CCDC115 to, among others, COPI vesicles that are involved in ER-to-Golgi transport and sorting of cargo proteins, could indicate a similar mechanism.

Based on comparative genomics, it is likely that CCDC115 and the yeast protein Vma22p are orthologs and have, at least partially, overlapping functions. Vma22p is involved in assembly of the V-ATPase proton pump by stabilizing the V0 domain during early assembly in the ER. Vma22 knockout yeast showed diminished V-ATPase activity and destabilization of the V0 domain.[31] Possibly, mutations in *CCDC115* could exert part of the effect via alteration of V-ATPase assembly or function. Vma22p exerts its function as a V-ATPase assembly factor by interacting with Vph2p (also called Vma12p [GenBank: NP_012803]) and Vma21p (GenBank: NP_011619.3).[27] In another study in this issue, we have identified TMEM199 (also known as C17orf32 [GenBank: NP_689677.1]) as the human homolog of Vph2, and recently VMA21 (GenBank: NP_001017980.1) has been described as the human homolog of Vma21p.[32,33]

Individuals with TMEM199 deficiency showed partial clinical and biochemical overlap with CCDC115-deficient individuals, although symptoms seem to be milder. TMEM199-deficient individuals presented in adolescence with a phenotype of elevated ATs and ALP, hypercholesterolemia, hepatic steatosis, and low ceruloplasmin. Profound hepatosplenomegaly and PMD, as seen in CCDC115 deficiency, were absent. Compared to known V-ATPase-associated disorders, CCDC115 deficiency (and TMEM199 deficiency) is the first that predominantly affects the liver.[34] Mutations in *VMA21* cause X-linked myopathy with excessive autophagy (XMEA [MIM: 310440]). XMEA is a disorder associated with progressive muscle weakness.[35,36] Mutations in V-ATPase subunits *TCIRG1* (also called *ATP6V0A3*) and *ATP6V0A4* cause tissue-specific symptoms (osteopetrosis [MIM: 259700] and distal renal tubular acidosis [MIM: 602722]).[37,38] A hallmark clinical feature of ATP6V0A2-affected individuals is cutis laxa.[39] Biochemically, ATP6V0A2 deficiency is highly similar to CCDC115 (and TMEM199) deficiency with defective N- and O-glycosylation.[10,40] Interestingly, the most severely affected individual (F5-II1) was diagnosed with redundant skin and poor muscle volume, symptoms characteristic of ATP6V0A2 and VMA21 deficiency, respectively. This hints at a phenotypical continuum among several V-ATPase-associated disorders.

The storage-disease-like phenotype of CCDC115 deficiency resembles that of lysosomal disease, such as Niemann-Pick disease type C (NPC, caused by mutations in *NPC1* and *NPC2* [MIM: 257220]). NPC is characterized by hepatosplenomegaly and neurologic manifestations.[41] Lysosomal accumulation of cholesterol and sphingomyelin due to impaired cholesterol trafficking is the hallmark of NPC; hence, NPC can be regarded as a cholesterol trafficking disease.[42] NPC1 and NPC2 work in conjunction with each other and are involved in the transport of cholesterol from late endosomes and lysosomes to the plasma membrane and ER. Interestingly, binding of cholesterol to NPC2 is improved in an acidic environment, and this could be a possible link between CCDC115 deficiency and NPC, given that the V-ATPase is the main acidifier of lysosomal pH.[43] Alternatively, altered trafficking of lysosomal proteins could explain the clinical resemblance.

All individuals had elevated serum ALP on biochemical analysis. This was determined to be bone derived for the investigated individuals. Discrepantly high bone-derived ALP can be observed in individuals with defects of GPI anchor biosynthesis.[44,45] However, this is not supported for CCDC115 deficiency. Trafficking of GPI-anchored proteins, which might include ALP, is suggested to occur through a COPII-dependent process from ER exit sites.[46] In Vma22p mutant yeast, trafficking of ALP to the yeast vacuole is not majorly altered.[31] However, yeast ALP is membrane bound and not a GPI-anchored protein. Treatment of yeast with bafilomycin A1, a potent V-ATPase inhibitor known to block vacuole acidification, did not show any effect on trafficking and maturation of membrane-bound yeast ALP.[47] This suggests that transport of vacuolar membrane proteins, including ALP, in yeast is independent from acidification. A study in mouse pituitary corticotrope tumor cells showed decreased trafficking of cargo proteins, independent of pH, after incubation with Concamycin A (ConA), another V-ATPase inhibitor. Although knockdown of the V-ATPase showed an overlapping phenotype with ConA treatment, this was not investigated for protein secretion. Additionally, processing of the investigated protein, PC1, begins in the *trans*-Golgi network and could therefore not be representative for Golgi trafficking.[48] Based on the localization of CCDC115 in the ER-to-Golgi region, it could be speculated that CCDC115 has a role in protein cargo sorting or trafficking of alkaline phosphatase in addition to a possible role in V-ATPase assembly.

In conclusion, we describe eight individuals with a type 2 CDG from five unrelated families affected by mutations in *CCDC115*. The phenotype consists of elevated aminotransferases and alkaline phosphatase and hepatosplenomegaly in combination with psychomotor disability, hypercholesterolemia, and hypotonia. Based on homology detection, glycosylation studies, and cellular co-localization, we propose a role for CCDC115 in Golgi homeostasis.

Accession Numbers

The accession numbers for the pathogenic variants c.92T>C, c.31G>T, and c.92T>C and the *CCDC115* deletion reported in this paper are ClinVar: SCV000257472, SCV000257474, and SCV000257477, respectively.

Supplemental Data

Supplemental Data include two figures and seven tables and can be found with this article online at http://dx.doi.org/10.1016/j.ajhg.2015.12.010.

Acknowledgments

We would like to thank all individuals and their families for their participation in this study. We would also like to thank the group of Prof. C. Biot and Dr. Y. Guerardel for their generous donation of

ManNAI and Dr. F. Pellicano and Dr. T. Iwata for their generous donation of the anti-CCDC115 antisera. This work was financially supported by grants from the Institute of Genetic and Metabolic Disease (D.J.L., J.A.V., and R. J. Rodenburg), the Dutch Organization for Scientific Research (ZONMW Medium Investment grant 40-00506-98-9001, VIDI grant 91713359 to D.J.L., and VENI grant to A.G.H.), the AMC graduate school PhD scholarship (M.A.W.v.d.B.), the Metakids foundation (J.C.J., M.V.S., J.D., D.J.L.), the Dr. Karel-Lodewijk Verleysen Award (J.D.), the Spanish Ministry of Economy and Competitiveness (grant PI11/01254 to B.P., C.P.C., and C.M.), the German Research Foundation (S.C.), Muscular Dystrophy Association (S.C.), the French national agency (ANR-SOLV_CDG to F.F.), and the ERA-Net for Research Programs on Rare Diseases Joint Transnational Call 2011 (EURO-CDG, grant ERARE11-135 to G.M. and F.F.).

Received: July 9, 2015
Accepted: December 11, 2015
Published: January 28, 2016

Web Resources

The URLs for data presented herein are as follows:

BLAST, http://blast.ncbi.nlm.nih.gov/Blast.cgi
COILS, http://www.ch.embnet.org/software/COILS_form.html
dbSNP, http://www.ncbi.nlm.nih.gov/projects/SNP/
ExAC Browser, http://exac.broadinstitute.org
ImageJ, http://imagej.nih.gov/ij
Jalview, http://www.jalview.org
MutationTaster, http://www.mutationtaster.org/
OMIM, http://www.omim.org/
PolyPhen-2, http://genetics.bwh.harvard.edu/pph2/
SIFT, http://sift.jcvi.org
SNPcheck, https://secure.ngrl.org.uk/SNPCheck/snpcheck.htm
TISGolgi, tisbio.wix.com/tisbio
UCSC Human Genome Browser, http://genome-euro.ucsc.edu/index.html

References

1. Freeze, H.H., Chong, J.X., Bamshad, M.J., and Ng, B.G. (2014). Solving glycosylation disorders: fundamental approaches reveal complicated pathways. Am. J. Hum. Genet. *94*, 161–175.
2. Ng, B.G., Buckingham, K.J., Raymond, K., Kircher, M., Turner, E.H., He, M., Smith, J.D., Eroshkin, A., Szybowska, M., Losfeld, M.E., et al.; University of Washington Center for Mendelian Genomics (2013). Mosaicism of the UDP-galactose transporter SLC35A2 causes a congenital disorder of glycosylation. Am. J. Hum. Genet. *92*, 632–636.
3. Guillard, M., Morava, E., de Ruijter, J., Roscioli, T., Penzien, J., van den Heuvel, L., Willemsen, M.A., de Brouwer, A., Bodamer, O.A., Wevers, R.A., et al. (2011). B4GALT1-congenital disorders of glycosylation presents as a non-neurologic glycosylation disorder with hepatointestinal involvement. J pediatr. *159*, 1041–1043 e1042.
4. Tan, J., Dunn, J., Jaeken, J., and Schachter, H. (1996). Mutations in the MGAT2 gene controlling complex N-glycan synthesis cause carbohydrate-deficient glycoprotein syndrome type II, an autosomal recessive disease with defective brain development. Am. J. Hum. Genet. *59*, 810–817.
5. Miller, V.J., and Ungar, D. (2012). Re'COG'nition at the Golgi. Traffic *13*, 891–897.
6. Foulquier, F., Amyere, M., Jaeken, J., Zeevaert, R., Schollen, E., Race, V., Bammens, R., Morelle, W., Rosnoblet, C., Legrand, D., et al. (2012). TMEM165 deficiency causes a congenital disorder of glycosylation. Am. J. Hum. Genet. *91*, 15–26.
7. Demaegd, D., Foulquier, F., Colinet, A.S., Gremillon, L., Legrand, D., Mariot, P., Peiter, E., Van Schaftingen, E., Matthijs, G., and Morsomme, P. (2013). Newly characterized Golgi-localized family of proteins is involved in calcium and pH homeostasis in yeast and human cells. Proc. Natl. Acad. Sci. USA *110*, 6859–6864.
8. Kornak, U., Reynders, E., Dimopoulou, A., van Reeuwijk, J., Fischer, B., Rajab, A., Budde, B., Nürnberg, P., Foulquier, F., Lefeber, D., et al.; ARCL Debré-type Study Group (2008). Impaired glycosylation and cutis laxa caused by mutations in the vesicular H+-ATPase subunit ATP6V0A2. Nat. Genet. *40*, 32–34.
9. Forgac, M. (2007). Vacuolar ATPases: rotary proton pumps in physiology and pathophysiology. Nat. Rev. Mol. Cell Biol. *8*, 917–929.
10. Hucthagowder, V., Morava, E., Kornak, U., Lefeber, D.J., Fischer, B., Dimopoulou, A., Aldinger, A., Choi, J., Davis, E.C., Abuelo, D.N., et al. (2009). Loss-of-function mutations in ATP6V0A2 impair vesicular trafficking, tropoelastin secretion and cell survival. Hum. Mol. Genet. *18*, 2149–2165.
11. Marshansky, V., Rubinstein, J.L., and Grüber, G. (2014). Eukaryotic V-ATPase: novel structural findings and functional insights. Biochim. Biophys. Acta *1837*, 857–879.
12. Wopereis, S., Grünewald, S., Huijben, K.M., Morava, E., Mollicone, R., van Engelen, B.G., Lefeber, D.J., and Wevers, R.A. (2007). Transferrin and apolipoprotein C-III isofocusing are complementary in the diagnosis of N- and O-glycan biosynthesis defects. Clin. Chem. *53*, 180–187.
13. Wopereis, S., Grünewald, S., Morava, E., Penzien, J.M., Briones, P., García-Silva, M.T., Demacker, P.N., Huijben, K.M., and Wevers, R.A. (2003). Apolipoprotein C-III isofocusing in the diagnosis of genetic defects in O-glycan biosynthesis. Clin. Chem. *49*, 1839–1845.
14. van Scherpenzeel, M., Steenbergen, G., Morava, E., Wevers, R.A., and Lefeber, D.J. (2015). High-resolution mass spectrometry glycoprofiling of intact transferrin for diagnosis and subtype identification in the congenital disorders of glycosylation. Transl. Res. *166*, 639–649.
15. Stránecký, V., Hoischen, A., Hartmannová, H., Zaki, M.S., Chaudhary, A., Zudaire, E., Nosková, L., Barešová, V., Přistoupilová, A., Hodaňová, K., et al. (2013). Mutations in ANTXR1 cause GAPO syndrome. Am. J. Hum. Genet. *92*, 792–799.
16. Vissers, L.E., de Ligt, J., Gilissen, C., Janssen, I., Steehouwer, M., de Vries, P., van Lier, B., Arts, P., Wieskamp, N., del Rosario, M., et al. (2010). A de novo paradigm for mental retardation. Nat. Genet. *42*, 1109–1112.
17. Untergasser, A., Cutcutache, I., Koressaar, T., Ye, J., Faircloth, B.C., Remm, M., and Rozen, S.G. (2012). Primer3–new capabilities and interfaces. Nucleic Acids Res. *40*, e115.
18. Koressaar, T., and Remm, M. (2007). Enhancements and modifications of primer design program Primer3. Bioinformatics *23*, 1289–1291.
19. White, S.J., Vink, G.R., Kriek, M., Wuyts, W., Schouten, J., Bakker, B., Breuning, M.H., and den Dunnen, J.T. (2004). Two-color multiplex ligation-dependent probe amplification: detecting genomic rearrangements in hereditary multiple exostoses. Hum. Mutat. *24*, 86–92.
20. Birnboim, H.C., and Doly, J. (1979). A rapid alkaline extraction procedure for screening recombinant plasmid DNA. Nucleic Acids Res. *7*, 1513–1523.

21. Guillard, M., Wada, Y., Hansikova, H., Yuasa, I., Vesela, K., Ondruskova, N., Kadoya, M., Janssen, A., Van den Heuvel, L.P., Morava, E., et al. (2011). Transferrin mutations at the glycosylation site complicate diagnosis of congenital disorders of glycosylation type I. J. Inherit. Metab. Dis. *34*, 901–906.
22. Guillard, M., Morava, E., van Delft, F.L., Hague, R., Körner, C., Adamowicz, M., Wevers, R.A., and Lefeber, D.J. (2011). Plasma N-glycan profiling by mass spectrometry for congenital disorders of glycosylation type II. Clin. Chem. *57*, 593–602.
23. Vanbeselaere, J., Vicogne, D., Matthijs, G., Biot, C., Foulquier, F., and Guerardel, Y. (2013). Alkynyl monosaccharide analogues as a tool for evaluating Golgi glycosylation efficiency: application to Congenital Disorders of Glycosylation (CDG). Chem. Commun. (Camb.) *49*, 11293–11295.
24. Mohamed, M., Guillard, M., Wortmann, S.B., Cirak, S., Marklova, E., Michelakakis, H., Korsch, E., Adamowicz, M., Koletzko, B., van Spronsen, F.J., et al. (2011). Clinical and diagnostic approach in unsolved CDG patients with a type 2 transferrin pattern. Biochim. Biophys. Acta *1812*, 691–698.
25. Altschul, S.F., Madden, T.L., Schäffer, A.A., Zhang, J., Zhang, Z., Miller, W., and Lipman, D.J. (1997). Gapped BLAST and PSI-BLAST: a new generation of protein database search programs. Nucleic Acids Res. *25*, 3389–3402.
26. Ho, M.N., Hill, K.J., Lindorfer, M.A., and Stevens, T.H. (1993). Isolation of vacuolar membrane H(+)-ATPase-deficient yeast mutants; the VMA5 and VMA4 genes are essential for assembly and activity of the vacuolar H(+)-ATPase. J. Biol. Chem. *268*, 221–227.
27. Graham, L.A., Hill, K.J., and Stevens, T.H. (1998). Assembly of the yeast vacuolar H+-ATPase occurs in the endoplasmic reticulum and requires a Vma12p/Vma22p assembly complex. J. Cell Biol. *142*, 39–49.
28. Szklarczyk, R., Wanschers, B.F., Cuypers, T.D., Esseling, J.J., Riemersma, M., van den Brand, M.A., Gloerich, J., Lasonder, E., van den Heuvel, L.P., Nijtmans, L.G., and Huynen, M.A. (2012). Iterative orthology prediction uncovers new mitochondrial proteins and identifies C12orf62 as the human ortholog of COX14, a protein involved in the assembly of cytochrome c oxidase. Genome Biol. *13*, R12.
29. Pellicano, F., Inglis-Broadgate, S.L., Pante, G., Ansorge, W., and Iwata, T. (2006). Expression of coiled-coil protein 1, a novel gene downstream of FGF2, in the developing brain. Gene Expr. Patterns *6*, 285–293.
30. Pellicano, F., Thomson, R.E., Inman, G.J., and Iwata, T. (2010). Regulation of cell proliferation and apoptosis in neuroblastoma cells by ccp1, a FGF2 downstream gene. BMC Cancer *10*, 657.
31. Hill, K.J., and Stevens, T.H. (1995). Vma22p is a novel endoplasmic reticulum-associated protein required for assembly of the yeast vacuolar H(+)-ATPase complex. J. Biol. Chem. *270*, 22329–22336.
32. Ramachandran, N., Munteanu, I., Wang, P., Ruggieri, A., Rilstone, J.J., Israelian, N., Naranian, T., Paroutis, P., Guo, R., Ren, Z.P., et al. (2013). VMA21 deficiency prevents vacuolar ATPase assembly and causes autophagic vacuolar myopathy. Acta Neuropathol. *125*, 439–457.
33. Jansen, J.C., Timal, S., Van Scherpenzeel, M., Michelakakis, H., Vicogne, D., Moraitou, M., Hoischen, A., Huijben, K., Steenbergen, G., van den Boogaard, M.A.W., et al. (2015). TMEM199 deficiency causes a Golgi homeostasis disorder characterized by elevated aminotransferases, alkaline phosphatase, and cholesterol and abnormal glycosylation. Am. J. Hum. Genet. *98*, this issue, 322–330.
34. Janssen, M.J., Waanders, E., Woudenberg, J., Lefeber, D.J., and Drenth, J.P. (2010). Congenital disorders of glycosylation in hepatology: the example of polycystic liver disease. J. Hepatol. *52*, 432–440.
35. Mercier, S., Magot, A., Caillon, F., Isidor, B., David, A., Ferrer, X., Vital, A., Coquet, M., Penttilä, S., Udd, B., et al. (2015). Muscle magnetic resonance imaging abnormalities in X-linked myopathy with excessive autophagy. Muscle Nerve *52*, 673–680.
36. Ruggieri, A., Ramachandran, N., Wang, P., Haan, E., Kneebone, C., Manavis, J., Morandi, L., Moroni, I., Blumbergs, P., Mora, M., and Minassian, B.A. (2015). Non-coding VMA21 deletions cause X-linked myopathy with excessive autophagy. Neuromuscul. Disord. *25*, 207–211.
37. Frattini, A., Orchard, P.J., Sobacchi, C., Giliani, S., Abinun, M., Mattsson, J.P., Keeling, D.J., Andersson, A.K., Wallbrandt, P., Zecca, L., et al. (2000). Defects in TCIRG1 subunit of the vacuolar proton pump are responsible for a subset of human autosomal recessive osteopetrosis. Nat. Genet. *25*, 343–346.
38. Smith, A.N., Skaug, J., Choate, K.A., Nayir, A., Bakkaloglu, A., Ozen, S., Hulton, S.A., Sanjad, S.A., Al-Sabban, E.A., Lifton, R.P., et al. (2000). Mutations in ATP6N1B, encoding a new kidney vacuolar proton pump 116-kD subunit, cause recessive distal renal tubular acidosis with preserved hearing. Nat. Genet. *26*, 71–75.
39. Fischer, B., Dimopoulou, A., Egerer, J., Gardeitchik, T., Kidd, A., Jost, D., Kayserili, H., Alanay, Y., Tantcheva-Poor, I., Mangold, E., et al. (2012). Further characterization of ATP6V0A2-related autosomal recessive cutis laxa. Hum. Genet. *131*, 1761–1773.
40. Guillard, M., Dimopoulou, A., Fischer, B., Morava, E., Lefeber, D.J., Kornak, U., and Wevers, R.A. (2009). Vacuolar H+-ATPase meets glycosylation in patients with cutis laxa. Biochim. Biophys. Acta *1792*, 903–914.
41. Vanier, M.T. (2010). Niemann-Pick disease type C. Orphanet J. Rare Dis. *5*, 16.
42. Vanier, M.T. (2015). Complex lipid trafficking in Niemann-Pick disease type C. J. Inherit. Metab. Dis. *38*, 187–199.
43. Storch, J., and Xu, Z. (2009). Niemann-Pick C2 (NPC2) and intracellular cholesterol trafficking. Biochim. Biophys. Acta *1791*, 671–678.
44. Howard, M.F., Murakami, Y., Pagnamenta, A.T., Daumer-Haas, C., Fischer, B., Hecht, J., Keays, D.A., Knight, S.J., Kölsch, U., Krüger, U., et al. (2014). Mutations in PGAP3 impair GPI-anchor maturation, causing a subtype of hyperphosphatasia with mental retardation. Am. J. Hum. Genet. *94*, 278–287.
45. Krawitz, P.M., Murakami, Y., Hecht, J., Krüger, U., Holder, S.E., Mortier, G.R., Delle Chiaie, B., De Baere, E., Thompson, M.D., Roscioli, T., et al. (2012). Mutations in PIGO, a member of the GPI-anchor-synthesis pathway, cause hyperphosphatasia with mental retardation. Am. J. Hum. Genet. *91*, 146–151.
46. Muñiz, M., and Zurzolo, C. (2014). Sorting of GPI-anchored proteins from yeast to mammals–common pathways at different sites? J. Cell Sci. *127*, 2793–2801.
47. Klionsky, D.J., and Emr, S.D. (1989). Membrane protein sorting: biosynthesis, transport and processing of yeast vacuolar alkaline phosphatase. EMBO J. *8*, 2241–2250.
48. Sobota, J.A., Bäck, N., Eipper, B.A., and Mains, R.E. (2009). Inhibitors of the V0 subunit of the vacuolar H+-ATPase prevent segregation of lysosomal- and secretory-pathway proteins. J. Cell Sci. *122*, 3542–3553.